Experimental investigations of air entrainment in transition and skimming flows down a stepped chute

H. Chanson and L. Toombes

Abstract: Stepped spillways have been used for about 3500 years. The last few decades have seen the development of new construction materials, design techniques, and applications, for example, embankment overtopping protection systems. Although it is commonly acknowledged that free-surface aeration is significant in stepped chutes, experimental data are scarce, often limited to very steep slopes ($\alpha \sim 50°$). This paper presents an experimental study conducted in a large-size stepped chute ($\alpha = 22°$, $h = 0.1$ m, $W = 1$ m). Observations demonstrate the existence of a transition flow pattern for intermediate flow rates between nappe and skimming flows. Detailed air–water flow measurements were conducted in both transition and skimming flows, immediately downstream of the inception point of free-surface aeration where uniform equilibrium flow conditions were not achieved. In skimming flows, a complete characterization is developed for the distributions of void fraction, bubble count rate, and velocity, and flow resistance data are compared with other studies. Transition flows exhibit significantly different air–water flow properties. They are highly aerated, requiring the design of comparatively high chute sidewalls.

Key words: stepped spillway, air entrainment, two-phase flow properties, skimming flow, transition flow.

Résumé : Les déversoirs en escalier ont été utilisés depuis plus de 3500 ans. Les quelques dernières décennies ont vu apparaître le développement de nouveaux matériaux de construction, techniques de conception et d'applications : e.g., systèmes de protection contre le débordements des barrages en remblai. Bien qu'il soit fréquemment reconnu que l'aération en surface libre est importante dans les déversoirs en escalier, les données expérimentales sont rares, se limitant souvent à des pentes raides ($\alpha \sim 50°$). Cet article présente une étude expérimentale conduite dans un grand déversoir en escalier ($\alpha = 22°$, $h = 0.1$ m, $W = 1$ m). Les observations démontrent l'existence d'un comportement d'écoulement de transition pour les débits moyens entre l'écoulement en nappe et l'écoulement extrêmement turbulent. Des mesures détaillées du débit air–eau ont été prises pour l'écoulement de transition et l'écoulement extrêmement turbulent, directement en aval du point d'aération en surface libre où des conditions d'écoulement uniforme à l'équilibre n'ont pas été achevées. Pour l'écoulement extrêmement turbulent, une caractérisation complète est développée pour les distributions des fractions de vides, le compte des bulles et leur vélocité, et les données de la résistance du débit sont comparées avec d'autres études. Les écoulements de transition montrent des différences significatives dans les propriétés de débit air–eau. Ils sont grandement aérés, ce qui demande une conception des murs de déversoir plus haut.

Mots clés : déversoir en escalier, entraînement d'air, propriétés des écoulements à deux phases, écoulement extrêmement turbulent, écoulement de transition.

[Traduit par la Rédaction]

1. Introduction

Stepped spillways have been used for about 3500 years (Chanson 2000). During the 19th century, the design technique was common in Europe, North America, and Australia (Schuyler 1909; Wegmann 1911; Kelen 1933; Chanson 1997*a*). By the end of the 19th century, it was understood that stepped chutes contributed significantly to the dissipation of the hydraulic energy, for example, the design of the Gold Creek and New Croton dam spillways (Wegmann 1907; Chanson and Whitmore 1998). The interest in stepped cascades dropped, however, during the first half of the 20th century with new progresses in the energy dissipation characteristics of hydraulic jumps favouring the design of hydraulic jump stilling basins. Stilling basins allowed larger energy dissipation and smaller structures, leading to cheaper construction cost.

Since the 1970s, the regain of interest for the stepped spillway design has been associated with the development of new construction materials (e.g., roller compacted concrete (RCC), polymer coated gabions), the introduction of new design techniques (e.g., overflow embankment dam protection systems with RCC and precast concrete blocks), and the de-

Received 6 June 2001. Revised manuscript accepted 20 November 2001. Published on the NRC Research Press Web site at http://cjce.nrc.ca on 10 February 2002.

H. Chanson[1] and L. Toombes. Department of Civil Engineering, The University of Queensland, Brisbane QLD 4072, Australia.

Written discussion of this article is welcomed and will be received by the Editor until 30 June 2002.

[1]Corresponding author (e-mail: h.chanson@mailbox.uq.edu.au).

 DOI: 10.1139/L01-084

velopment of new applications (e.g., re-oxygenation cascades). Research on stepped chute hydraulics has been very active: one book, 16 journal papers, and 26 discussions listed in Global Books in Print™ and Science Citation Index™ for the period 1985–2000. However, most studies prior to 1992 neglected the effects of free-surface aeration ("white waters"), until the first data by Ruff and Frizell (1994) and the analysis of Chanson (1993*a*). Today, experimental data on air entrainment down stepped chute are scarce, often limited to steep slopes ($\alpha \sim 50°$) as used for gravity dams. There is no data for slopes less than 25° that may be typical for embankment dam spillways.

It is the purpose of this study to provide a comprehensive database on air–water flows down stepped chutes. Measurements were conducted on a large facility ($\alpha = 22°$, $h = 0.1$ m, $W = 1$ m) with precise instrumentation. Based upon a Froude similitude, the large size of the facility ensures that the experimental results may be up-scaled with negligible scale effects for geometric scaling ratios less than 10:1. Two flow regimes were investigated, providing a broad spectrum of flow conditions. A complete characterization of the air–water flow properties is also provided.

2. Experimental apparatus and instrumentation

Experiments were conducted at the University of Queensland in a 2.7 m long, 1 m wide, 21.8° slope chute (Fig. 1). Waters were supplied from a large feeding basin (1.5 m deep, surface area 6.8 m × 4.8 m) leading to a sidewall convergent with a 4.8:1 contraction ratio. The test section consisted of a broad-crested weir (1 m wide, 0.6 m long, with upstream rounded corner (0.057 m radius)) followed by nine identical steps ($h = 0.1$ m, $l = 0.25$ m) made of marine ply. The stepped chute was 1 m wide with perspex sidewalls, followed by a horizontal concrete-invert canal ending in a dissipation pit.

The flow rate was delivered by a pump controlled with an adjustable frequency AC motor drive, enabling an accurate discharge adjustment in a closed-circuit system. The discharge was measured from the upstream head above crest with an accuracy of about 2% (Ackers et al. 1978).

Clear-water flow depths were measured with a point gauge. Air–water flow properties were measured using two types of conductivity probe: a single-tip probe (Ø = 0.35 mm), and a double-tip probe (Ø = 0.025 mm). The probe sensors were aligned in the flow direction and excited by an air bubble detector (AS25240). The velocity measurements were the longitudinal component of the air–water interfacial velocity. The probe signal was scanned at 5 kHz for 180 s and at 20 kHz for 20 s for the single-tip and double-tip probes respectively. The translation of the probes in the direction normal to the channel invert was controlled by a fine adjustment travelling mechanism connected to a Mitutoyo™ digimatic scale unit (Ref. No. 572-503). The error on the vertical position of the probe was less than 0.025 mm. The accuracy on the longitudinal probe position was estimated as $\Delta x < \pm 0.5$ cm. The accuracy on the transverse position of the probe was less than 1 mm. Flow visualizations were conducted with a digital video-camera Sony™ DV-CCD DCR-TRV900 (speed: 25 fra/s, shutter: 1/4 to 1/10 000 s) and high-speed still photographs.

Experimental observations were conducted for flow rates ranging from 0.025 to 0.30 m^3/s. Detailed air–water flow properties were recorded for 19 flow rates ranging from 0.046 to 0.182 m^3/s (Table 1). Measurements were performed at the step edges, unless indicated (Fig. 1). Note that uniform equilibrium flow conditions were not achieved at the downstream end of the chute because the flume was relatively short. Further details of the experimental facility and of the results were reported by Chanson and Toombes (2001).

3. Basic flow patterns

3.1. Flow regime

The facility was designed to operate with flow conditions ranging from nappe to skimming flow regimes. For $d_c/h < 0.53$, where d_c is the critical depth and h is the step height, the water flowed down the chute as a succession of clear, distinct free-falling nappes referred to as the nappe flow regime. For $d_c/h > 0.97$, the flow skimmed over the pseudo-bottom formed by the step edges, that is, skimming flow regime (Figs. 1*a* and 1*b*). Intense cavity recirculation was observed at each step. For intermediate discharges ($0.53 < d_c/h < 0.97$), a transition flow pattern was observed. Dominant flow features of transition flows included strong splashing and droplet ejections at any position downstream of the inception point of free-surface aeration. Small to medium air cavities were observed irregularly. For example, a step with a small air pocket could be followed by a medium-size air cavity at the downstream step, followed by a tiny air cavity at the next drop. For an observer standing on the bank, the transition flow had a chaotic appearance with irregular droplet ejections that were seen to reach heights of up to 3–5 times the step height. It did not have the quasi-smooth free-surface appearance of skimming flows, nor the distinctive succession of free-falling nappes observed in nappe flows.

With both transition and skimming flows, the upstream flow was non-aerated and the free-surface exhibited an undular profile of same wavelength and in phase with the stepped invert profile. Free-surface instabilities were, however, observed (Fig. 1*c*). Similar wave instabilities were discussed by Anwar (1994) and Chanson (1997*b*). Anwar suggested that free-surface aeration may be initiated by free-surface wave development, while Chanson showed experimental evidence of free-surface aeration in partially developed flows.

Ohtsu and Yasuda (1997) were the first to mention the existence of a distinct "transition flow" regime between nappe and skimming flows. The present observations of changes in flow regime are close to their findings: $0.78 < d_c/h < 1.05$ for $\alpha = 18.4°$ (Yasuda and Ohtsu 1999). These are further consistent with previous reviews of nappe-to-skimming flow transition conditions (Rajaratnam 1990; Chanson 1996).

3.2. Inception of free-surface aeration

The location of the inception of free-surface aeration was clearly defined for each test, although cavity aeration was typically observed one to two steps upstream of the inception point (Figs. 1*a* and 1*b*). A similar observation was re-

Fig. 1. Photographs of the experimental facility: (*a*) definition sketch of the test section; (*b*) side view of a skimming flow (d_c/h = 1.5) from left to right; and (*c*) free-surface instabilities upstream of the inception point of free-surface aeration in a skimming flow, looking downstream (d_c/h = 1.16).

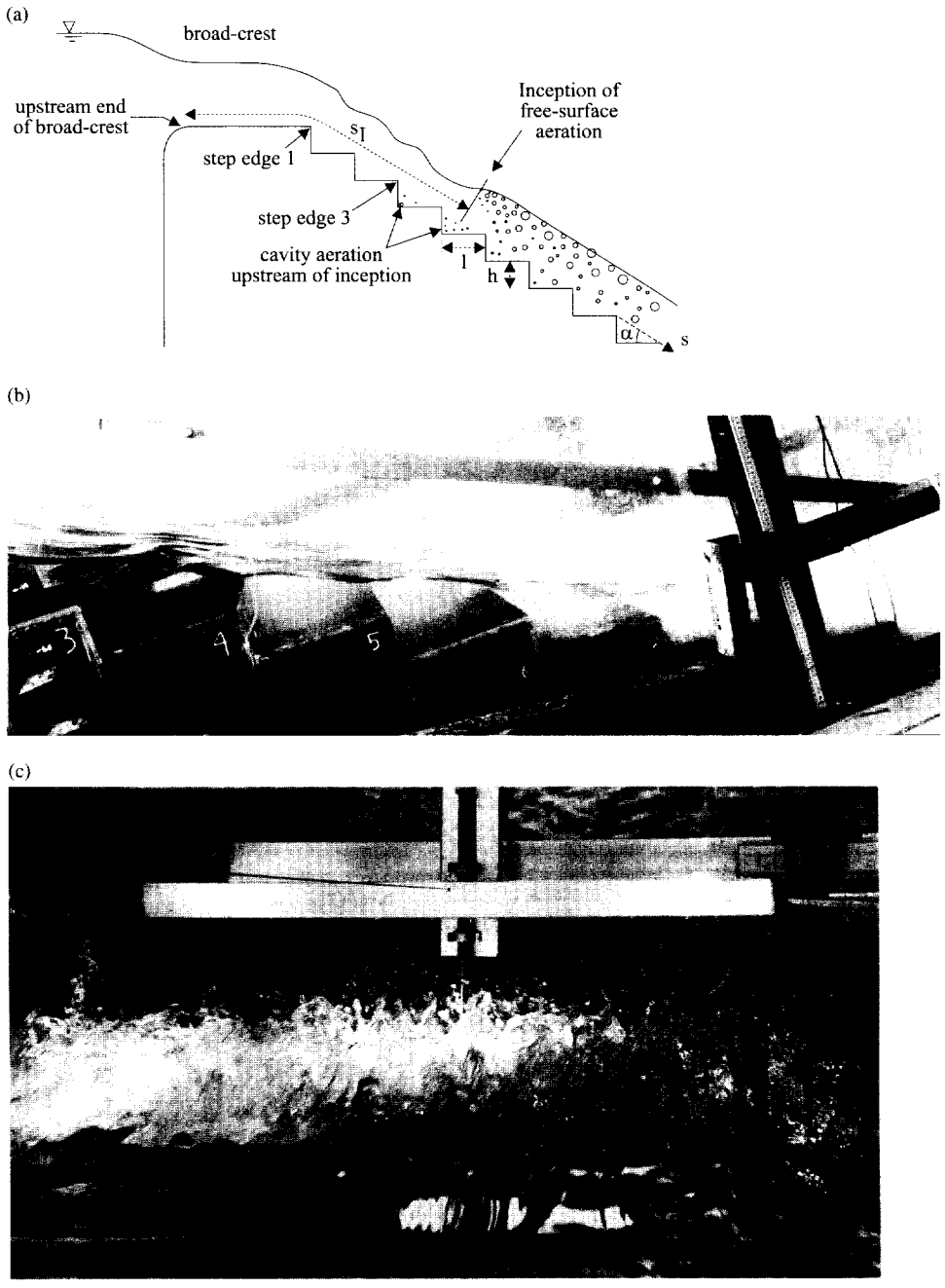

ported by Horner (1969), Chamani (2000), and Matos (2000).

Experimental observations of the longitudinal position of the inception point of free-surface aeration are reported in Fig. 2 as $s_I/(h \cos \alpha)$ as a function of F_* defined as

$$F_* = \frac{q_w}{\sqrt{g \sin \alpha (h \cos \alpha)^3}}$$

where h is the step height, α is the slope of the pseudo-bottom formed by the step edges, q_w is the water discharge per unit width, and s_I is the longitudinal distance measured from the upstream edge of the broad-crest. In Fig. 2, the data points (UQ 22°) regroup nappe flow ($F_* < 10$), transition flow ($10 < F_* < 18$), and skimming flow ($F_* > 18$) observations. They are compared with an incomplete set of observations (UQ 16°) obtained in the same flume with α = 16°, h = 0.1 m, and l = 0.35 m. Overall the data are best correlated by

$$[1] \qquad \frac{S_I}{h \cos \alpha} = \frac{12.34}{(\sin \alpha)^{0.0796}} \times F_*^{0.465}$$

for α = 15.9° and 21.9°, and $F_* < 3.8$. Experimental observations and eq. [1] are compared with skimming flow data

Table 1. Summary of experimental flow conditions for air–water flow measurements.

Ref. (1)	Q_w (m^3/s) (2)	Location of inception of free-surface aeration (3)	Flow regime (4)	Remarks (5)
Series 1				Single-tip probe
	0.182	Step edge 6	Skimming flow	Run Q5
	0.164	Step edge 6	Skimming flow	Run Q6
	0.147	Step edge 5	Skimming flow	Run Q7
	0.130	Step edge 5	Skimming flow	Run Q8
	0.124	Step edge 5	Skimming flow	Run Q1
	0.114	Step edge 5	Skimming flow	Run Q9
	0.103	Step edge 4	Skimming flow	Run Q2
	0.099	Step edge 4	Transition flow	Run Q10
	0.085	Step edge 4	Transition flow	Run Q11
	0.080	Step edge 4	Transition flow	Run Q3
	0.071	Step edge 3	Transition flow	Run Q12
	0.066	Step edge 3	Transition flow	Run Q4
	0.064	Step edge 3	Transition flow	Run Q13
	0.058	Step edge 3	Transition flow	Run Q14
	0.052	Step edge 3	Transition flow	Run Q15
	0.046	Step edge 3	Transition flow	Run Q16
Series 2				Double-tip probe
	0.182	Step edge 6	Skimming flow	Run Q23
	0.114	Step edge 5	Skimming flow	Run Q21
	0.058	Step edge 3	Transition flow	Run Q22

Fig. 2. Characteristic location of the inception point of free-surface aeration: $s_I/(h \cos \alpha)$ as a function of F_*.

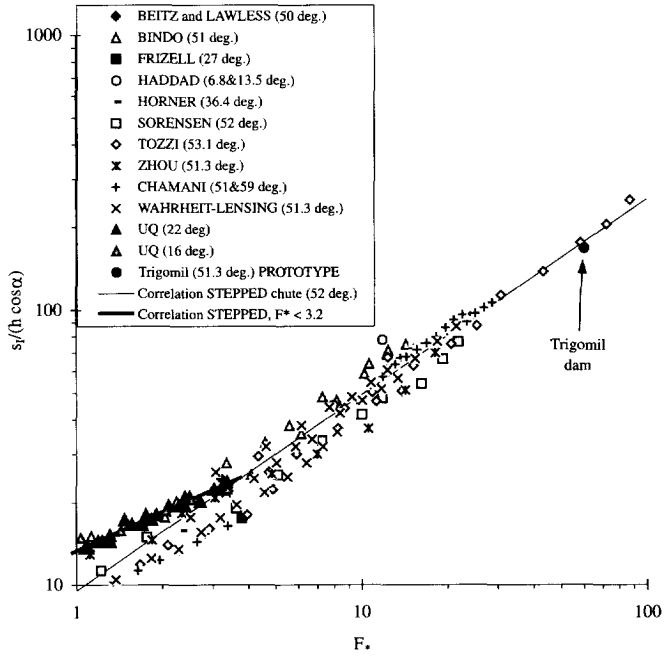

down steep chutes. The latter data set shows good agreement between laboratory and prototype observations, but they exhibit a trend that is best predicted by Chanson's (1995*a*) correlation for steep stepped chute and $F_* > 2$:

$$[2] \quad \frac{S_I}{h \cos \alpha} = \frac{19.72}{(\sin \alpha)^{0.0796}} \times F_*^{0.713}$$

4. Air–water flow properties in skimming flows

4.1. Basic air–water flow properties

Downstream of the inception point of free-surface aeration, a rapid free-surface aeration was observed. Air concentration distributions, measured at step edges, exhibited a smooth continuous profile. Experimental results are presented in Fig. 3 and compared with an analytical solution of the air bubble advective diffusion equation

$$[3] \quad C = 1 - \tanh^2\left[K'' - \frac{\frac{y}{Y_{90}}}{2D_o} + \frac{\left(\frac{y}{Y_{90}} - \frac{1}{3}\right)^3}{3D_o}\right]$$

(skimming flows)

where y is distance measured normal to the pseudo-bottom, Y_{90} is the characteristic distance where $C = 90\%$, K'' is an integration constant, and D_o is a function of the mean air concentration C_{mean} only (Appendix 1). A small number of measurements were taken half-distance between two step edges (Fig. 3*b*). The results suggest consistently a greater overall aeration than at adjacent step edges, with some aeration of the fluid layers next to the recirculation cavity (i.e., $y/Y_{90} < 0.3$).

Velocity distributions are presented in Fig. 3. At the step edges (Figs. 3*a* and 3*c*), the data follow the power law:

Fig. 3. Air–water flow properties in skimming flows (d_c/h = 1.5) — comparison with eqs. [3] and [4] — inception of free-surface aeration upstream of step edge 6: (*a*) flow conditions at the 7th step edge; (*b*) flow conditions half-distance between the 7th and 8th step edges; (*c*) flow conditions at the 8th step edge; and (*d*) dimensionless bubble count rate distributions (data measured with single-tip probe) for d_c/h = 1.1 and comparison with eq. [5].

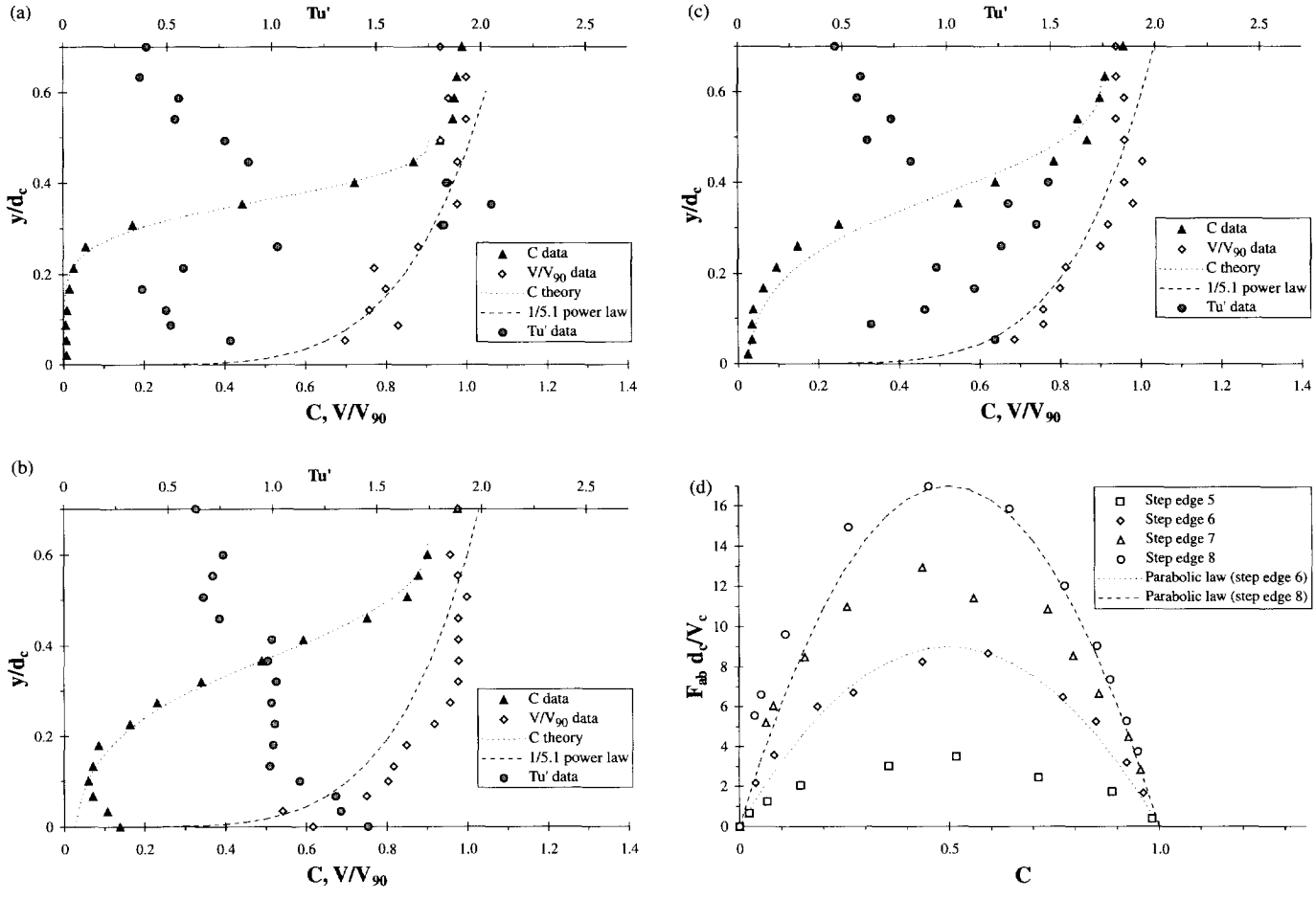

$$[4] \quad \frac{V}{V_{90}} = \left(\frac{y}{Y_{90}}\right)^{1/N}$$

at step edges, where V_{90} is the characteristic velocity for C = 90%. N was found to be about 5.1 and 6.0 for d_c/h = 1.5 and 1.1 respectively. Chanson (1995*a*) found N = 3.5 and 4 for the earlier works of Frizell (1992) and Tozzi (1992) respectively. Matos (2000) performed air–water velocity measurements in a longer chute and observed N ~ 4. In the present study, the flume was relatively short and uniform equilibrium flow conditions were not achieved. This might account for some difference with Matos' results while he used a flushed Pitot tube, which is not accurate at high void fractions. Between step edges, the velocity distribution was affected by the cavity recirculation and did not follow eq. [4] (Fig. 3*b*).

Figure 3*d* presents dimensionless distributions of bubble count rates $F_{ab}d_c/V_c$, where F_{ab}, the bubble count rate or bubble frequency, is defined as the number of bubbles impacting the probe tip per second, d_c is the critical depth, and V_c is the critical flow velocity. For a given flow velocity and void fraction, the bubble count rate F_{ab} is inversely proportional to the mean bubble size and directly proportional to the air–water specific interface area. The relationship between the bubble frequency and air content exhibits a characteristic parabolic shape, which is best fitted by

$$[5] \quad \frac{F_{ab}}{(F_{ab})_{max}} = 4C(1-C)$$

with the maximum bubble frequency $(F_{ab})_{max}$ for C ~ 50%.

4.2. Turbulent velocity field

Distributions of modified turbulence intensity Tu′ are presented in Fig. 3. The data were measured with the dual-tip resistivity probe and details of the processing technique, including the definition of Tu′, are given in Appendix 2. Although Tu′ is not exactly equal to the turbulence intensity, it provides some information on the turbulence level in the flow. Figure 3 includes data measured at step edges (Figs. 3*a* and 3*c*) and in between step edges (Fig. 3*b*).

In Fig. 3 the distributions of turbulence intensity Tu′ exhibit relatively uniform profiles implying high turbulence levels across the entire air–water flow mixture ($0 \leq y/Y_{90} \leq 1$). The trend differs significantly from the well-known turbulence intensity profiles observed in turbulent boundary layers (Schlichting 1979). On stepped chutes, it is believed

that the high rate of energy dissipation, associated with form drag, contributes to strong turbulent mixing throughout the entire flow. Greater turbulence levels are expected within the developing shear layers, that is, in the wake of each step edge. Despite some scatter, the trend is observed for the lower regions (y/Y_{90} < 0.2 to 0.3) (Fig. 3*b*).

The quantitative values of turbulence intensity Tu′ are large (~100%). They are of the same order of magnitude as turbulence levels measured in separated flows past rectangular cavity (Haugen and Dhanak 1966), in wakes between large stones (Sumer et al. 2001), and in the developing shear region of plunging water jets (Chanson and Brattberg 1998).

4.3. Comparison of void fraction profiles between smooth- and stepped-invert chute flows

Although the distribution of air concentration follows a trend similar to that seen in smooth-invert chute flows, small differences were consistently observed. This is highlighted in Fig. 4 with a comparison of void fraction distributions obtained for identical mean air concentration. Black symbols are prototype smooth-invert chute data at Aviemore dam spillway (Cain 1978) and the cross symbols are stepped chute data (present study). The skimming flow data are compared with eq. [3], and smooth chute data are compared with Chanson's (1995*b*) model developed and validated for smooth chute flows:

$$[6] \qquad C = 1 - \tanh^2\left(K' - \frac{y/Y_{90}}{2D'}\right) \qquad \text{(self - aerated flows)}$$

where the integration constant K' and the dimensionless air bubble diffusivity D' are functions of the mean air content only (Appendix 1).

The comparison of void fraction profiles indicates that, for an identical mean air content, skimming flows are more aerated in the upper flow layer (C > 0.3 to 0.5) than in smooth-invert self-aerated flows, and lesser air is observed in the lower layers (Fig. 4). A similar trend was observed with the stepped chute data of Tozzi et al. (1998). The result suggests a stronger droplet ejection mechanism in skimming flows, whereby water ejections reach comparatively higher elevations (than in smooth chute flows) before re-attaching to the flow. The trend must be related to different turbulent processes, that is, skin friction in smooth-invert chutes versus form drag in skimming flow down stepped chutes.

5. Air–water flow properties in transition flows

Free-surface aeration was found to be very intense for all transition flow rates. Downstream of the inception point of free-surface aeration, mean air concentrations ranged from 0.2 to 0.6 typically, with maximum mean air content of up to 78% measured at one step edge. Major redistributions of air content and velocity were observed between adjacent, successive step edges. Similar longitudinal fluctuations of flow properties were observed in transition flows down a 3.4° stepped chute (h = 0.071 and 0.143 m) at the University of Queensland, suggesting that the finding is not specific to the

Fig. 4. Comparison of air concentration distributions in smooth-invert and stepped chute flows: (*a*) C_{mean} = 0.27 and (*b*) C_{mean} = 0.35. (Smooth-invert data: black symbols, solid line (eq. [6]); stepped chute data: cross symbols, dashed line (eq. [3]).)

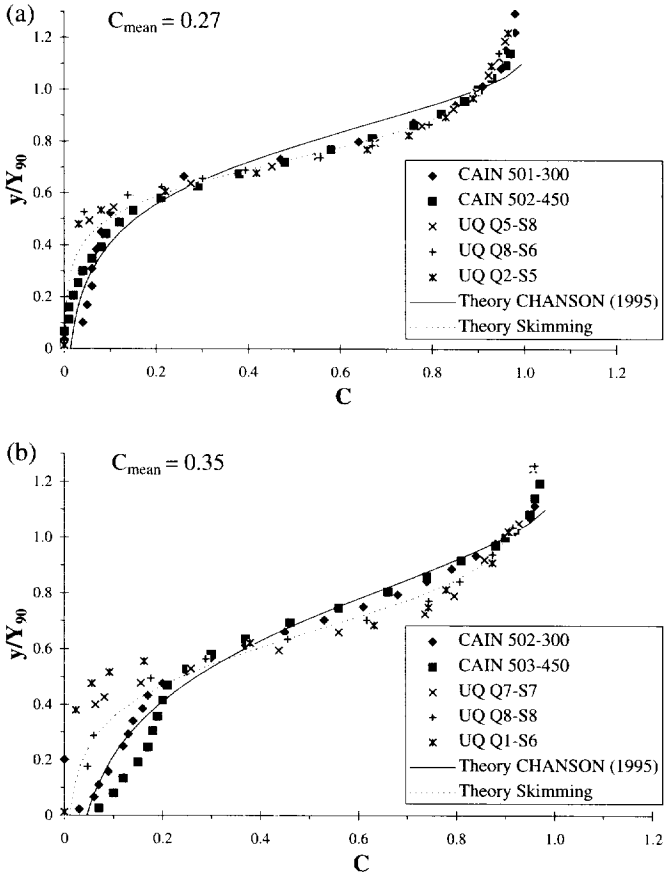

facility. Figure 5 shows air–water flow properties for one typical flow rate.

At most step edges, the distributions of air concentration may be fitted by

$$[7] \qquad C = K'''\left[1 - \exp\left(-\lambda \frac{y}{Y_{90}}\right)\right]$$

where K''' and λ are functions of the mean air content only (Appendix 1). Equation [7] compares favourably with most data, except for the first step edge downstream of the inception point of free-surface aeration and for the deflecting jet flow (Fig. 5).

For most flow rates, a deflecting flow was observed a few steps downstream of the inception point of free-surface aeration. Visually, the flow appeared to bypass one step, barely touching the step edge. At that step, liquid fractions (1 – C) greater than 10% were measured at distances up to 1.5d_c and some spray overtopped the 1.25 m high sidewalls. The nappe reattached the main flow at the next downstream step. In Fig. 5, such a deflected nappe is seen at the 6th step edge (Fig. 5*d*). For d_c/h < 0.8, the deflecting flow was consistently observed at the 4th step edge downstream of the inception of free-surface aeration. At the lowest flow rates, a

Fig. 5. Comparison of experimental and theoretical (eq. [7]) results of dimensionless air concentration and velocity distributions in a transition flow (Q_w = 0.058 m^3/s): (*a*) at the 3rd step edge, immediately downstream of the inception point of free-surface aeration; (*b*) at the 4th step edge; (*c*) at the 5th step edge; (*d*) at the 6th step edge (deflected nappe); (*e*) at the 7th step edge; and (*f*) at the 8th step edge (figure (*f*) also shows data for turbulent intensity distributions).

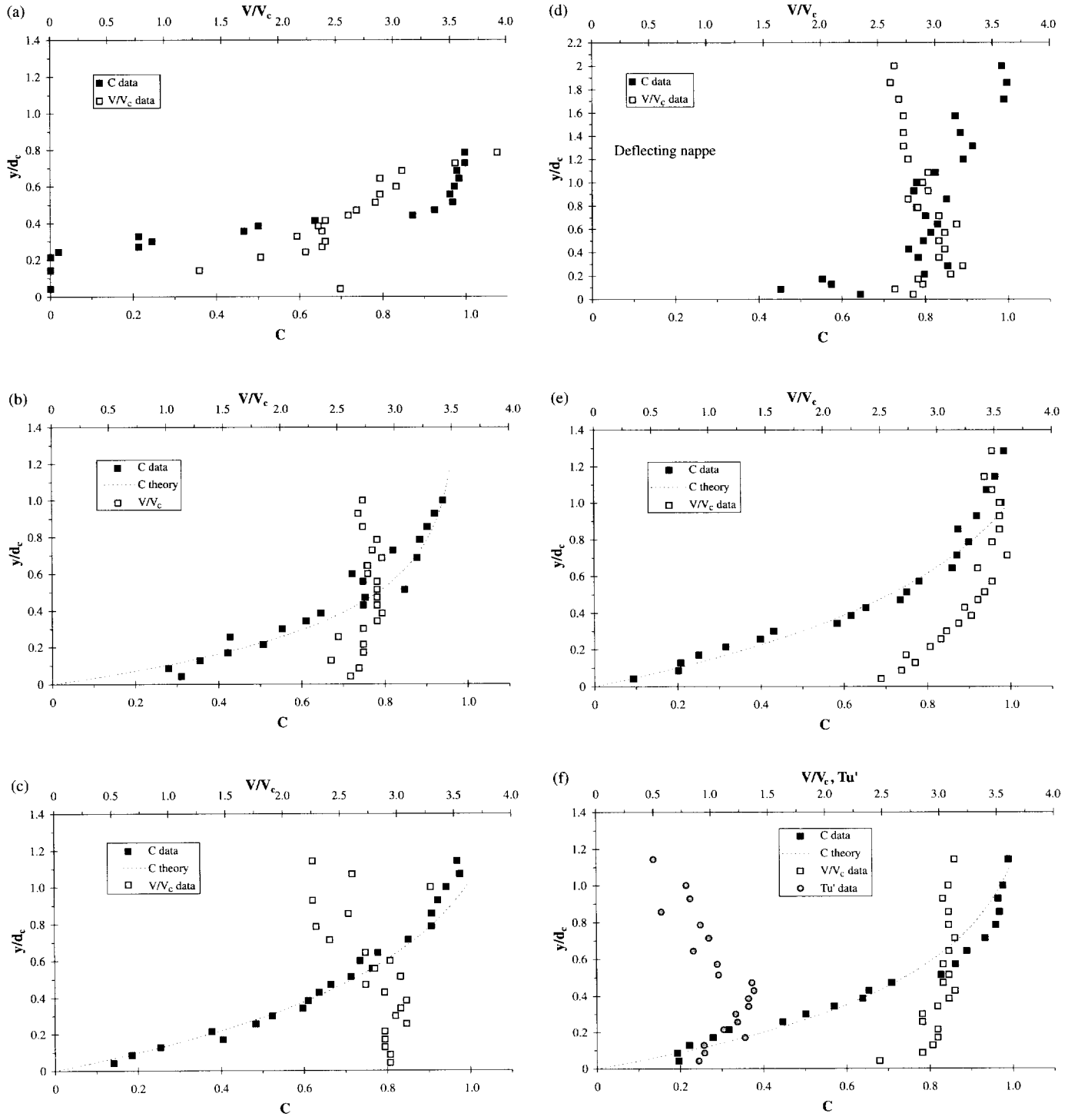

second deflecting flow was noted at the 6th step edge downstream of the inception point.

In transition flows, the distributions of bubble count rates follow about the parabolic law (eq. [5]) that was observed in smooth-invert chute flows and in skimming flows.

Air–water velocity distributions are presented in Fig. 5 as V/V_c versus y/d_c. Although, in a transition flow, the shape of the air concentration profiles is nearly identical for a given flow rate, the velocity distributions are rapidly varied from step edge to step edge (Fig. 5). The distributions of modified

Fig. 6. Longitudinal distributions of mean air content C_{mean} and dimensionless depth Y_{90}/d_c: (*a*) skimming flow data and comparison with numerical calculations (Wood 1985; Chanson 1993*b*); and (*b*) transition flow data.

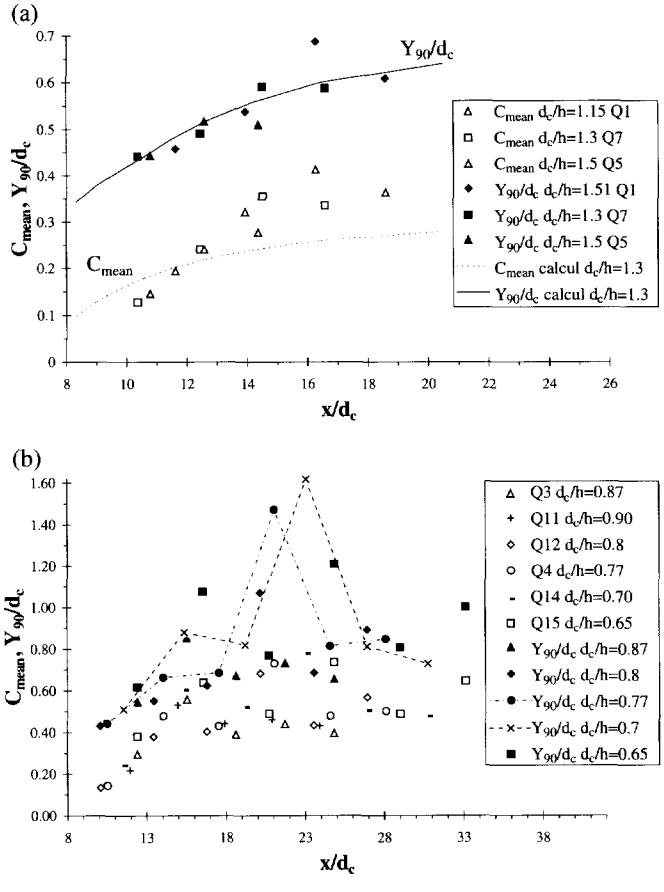

turbulence intensity Tu′ exhibit relatively uniform profiles across the air–water flow mixture (i.e., $0 \leq y/Y_{90} \leq 1$). Figure 5*f* shows an example. The quantitative values of turbulence intensity Tu′ are comparable with skimming flow data (Fig. 3).

5.1. Remarks

Equation [7] is an analytical solution of the diffusion equation (Appendix 1). It assumes that the air bubble diffusivity is zero for $C = 0$ and $C = 1$, and that it follows a distribution:

$$[8] \quad D' = \frac{C\sqrt{1-C}}{\lambda(K'-C)} \qquad \text{(transition flows)}$$

The shape is somehow similar to the sediment diffusivity distribution developed by Rouse (1937).

In a transition flow, the design of the sidewalls must account for the deflecting jet flows. That is, the chute sidewall height must be sized to at least $1.0Y_{90}$ (i.e., about $1.6d_c$), or even larger than $1.4Y_{90}$ if splashing is not acceptable, for example, with a road next to the spillway chute and high risks of frost and icy conditions. For comparison, Y_{90}/d_c was found to be less than 0.7–0.8 in skimming flows, during the present study (Fig. 6*b*).

6. Discussion

6.1. Air–water flow properties

Longitudinal distributions of mean air concentration C_{mean} and dimensionless air–water depth Y_{90}/d_c are presented in Fig. 6, where the horizontal axis x/d_c is the ratio of the distance from the downstream end of the broad crest to the critical depth. Note that the chute was relatively short and that uniform equilibrium flow conditions were not achieved at the downstream end.

In skimming flows, rapid aeration was observed at the inception point, followed by a gradual increase (Fig. 6*a*). In Fig. 6*a*, the data are compared with the numerical model developed for smooth-invert chutes by Wood (1985) and extended by Chanson (1993*b*). Calculations were conducted assuming a friction factor $f = 0.3$.

Transition flow data are presented in Fig. 6*b*. Note the different horizontal and vertical ranges between Figs. 6*a* and 6*b*. Very large aeration was observed in transition flows, in excess of acknowledged limits observed in smooth chute flows (Wood 1991; Chanson 1997*b*). The air–water flow depth data Y_{90} exhibited a saw-edged pattern, reaching up to 1.4–1.6 times d_c at deflected nappes. Overall, both sets of curves do not show a monotonic trend. Rather chaotic, irregular variations with increasing distances from the crest were observed. Similar instabilities were measured down a 3.4° stepped chute (h = 0.07 and 0.14 m) at the University of Queensland. Ohtsu and Yasuda[2] observed also the chaotic nature of transition flows for slopes ranging from 5.7° to 55°, although the "chaos" appeared more pronounced for $\alpha < 35°$.

Experimental results show that the maximum bubble frequency $(F_{ab})_{max}$ increased with longitudinal distance for each flow rate, and that it did not reach an upper limit within the length of the experimental channel. The test section was indeed relatively short and uniform equilibrium was not achieved at the downstream end. Figure 3*d* illustrates the longitudinal increase in maximum bubble frequency for a skimming flow.

6.2. Flow resistance in skimming flows

Skimming flows are characterized by significant form drag and form losses take place predominantly in the cavity recirculation. In gradually varied flows downstream of the inception point, the average shear stress between the skimming flow and the cavity recirculation may be calculated from the friction slope S_f (Henderson 1966). For a wide channel the energy equation yields

$$[9] \quad f_e = \frac{8\tau_o}{\rho_w U_w^2} = \frac{8g\left(\int_{y=0}^{y=Y_{90}} (1-C)\,dy\right)S_f}{U_w^2}$$

where the friction slope equals $S_f = -\partial H/\partial s$, H is the depth-averaged total head, s is the curvilinear coordinate along the

[2] Personal communication.

Table 2. Summary of experimental results of flow resistance in skimming flows.

Ref. (1)	Q_w (m^3/s) (2)	Flow regime (3)	f_e (3)	Remarks (4)
Series 1				Single-tip probe
	0.182	Skimming flow	0.143	Run Q5
	0.164	Skimming flow	0.157	Run Q6
	0.147	Skimming flow	0.196	Run Q7
	0.130	Skimming flow	0.184	Run Q8
	0.124	Skimming flow	0.215	Run Q1
	0.114	Skimming flow	0.283	Run Q9
	0.103	Skimming flow	0.157	Run Q2
	0.099	Transition flow	0.158	Run Q10
Series 2				Double-tip probe
	0.182	Skimming flow	0.092	Run Q23
	0.114	Skimming flow	0.074	Run Q21

Fig. 7. Flow resistance in skimming flow — comparison with eq. [10] (f_d = 0.2) and laboratory data obtained in large-size facilities (BaCaRa 1991; Shvainstein 1999; Chamani and Rajaratnam 1999; Yasuda and Ohtsu 1999; Matos 2000; Boes 2000; Present study (UQ 22°)).

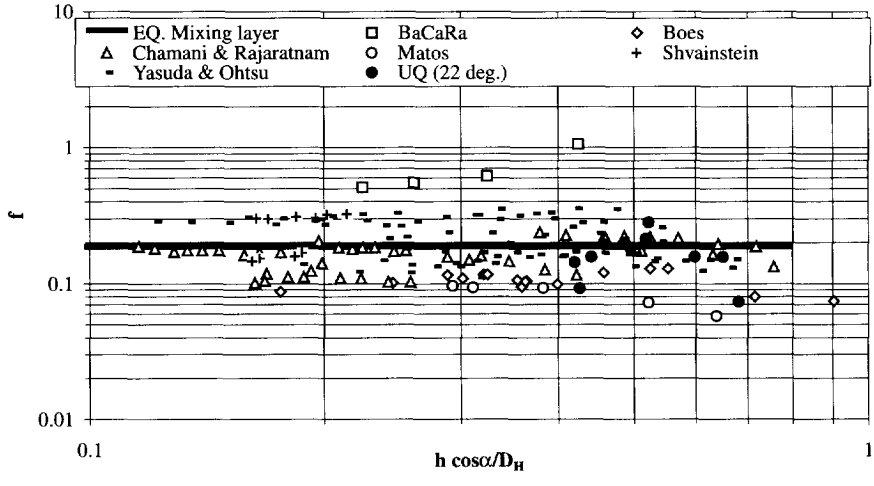

flow direction, f_e is the Darcy friction factor for air–water flow, and U_w is the mean water flow velocity ($U_w = q_w/d$). For the present series of experiments, the flow resistance was estimated using eq. [9] (Table 2). The data ranged from 0.093 to 0.28 within average f_e = 0.17. In Fig. 7, the present data are compared with skimming flow data obtained in large-size laboratory flumes (i.e., h > 0.02 m and Re > 1 × 10^5) for slopes ranging from 30 to 60°.

Overall, the friction factor data present no obvious correlation with the relative step roughness (h cos α/D_H), Reynolds, Froude, nor Weber numbers. However, they compare favourably with a simplified analytical model of the pseudo-boundary shear stress, which may be expressed, in dimensionless form, as

$$[10] \quad f_d = \frac{8\tau_o}{\rho_w U_w^2} = \frac{2}{\sqrt{\pi}}\left(\frac{1}{K}\right)$$

where f_d is an equivalent Darcy friction factor estimate of the form drag and $1/K$ is the dimensionless expansion rate of the shear layer (Chanson et al. 2000). Equation [10] predicts $f_d \approx 0.2$ for K = 6, i.e., close to the observed friction factors, particularly the present data (Fig. 7).

7. Conclusions

New experiments were conducted in a large-size stepped chute. Visual observations demonstrated three types of flow regimes: nappe flow, transition flow, and skimming flow. The transition flow regime was observed for a relatively broad range of flow rates. It was characterized by a chaotic flow motion, strong splashing, and very significant aeration.

Detailed air–water flow measurements were conducted in both transition and skimming flows immediately downstream of the inception point of free-surface aeration. In skimming flows, a complete characterization was developed for the distributions of void fraction, bubble count rate, and velocity. Although the air concentration distribution has the same shape as smooth chute flows, a slightly different trend was consistently observed, associated with strong droplet ejections. Flow resistance data are consistent with re-analysed data obtained in large-size laboratory chutes (Fig. 7). Transition flows exhibited significantly different air–water flow properties from those observed in skimming flows. For each experiment, a deflected nappe was observed occasionally (i.e., at one step). The deflected jet was highly

aerated and the associated spray would overtop the 1.25 m high sidewall.

Although the study was limited to one slope and for a short canal, the results highlighted the complexity of the free-surface aeration down stepped cascades down moderate slopes (i.e., $\alpha = 22°$ during the present study).

Acknowledgments

The writers thank Dr. John Macintosh, Water Solutions, and Professor Colin J. Apelt for helpful discussions and comments. They acknowledge the assistance of M. Eastman, N. Van Schagen, and G. Illidge (The University of Queensland).

References

Ackers, P., White, W.R., Perkins, J.A., and Harrison, A.J.M. 1978. Weirs and flumes for flow measurement. John Wiley, Chichester, U.K.

Anwar, H.O. 1994. Self-aerated flows on chutes and spillways — Discussion. ASCE Journal of Hydraulic Engineering, **120**(6): 778–779.

BaCaRa. 1991. Étude de la dissipation d'énergie sur les evacuateurs à marches. (Study of the energy dissipation on stepped spillways.) Report, Project National BaCaRa, CEMAGREF-SCP, October, Aix-en-Provence, France. (In French.)

Boes, R.M. 2000. Zweiphasenstroömung und Energieumsetzung auf Grosskaskaden. (Two-phase flow and energy dissipation on cascades.) Ph.D. thesis, VAW-ETH, Zürich, Switzerland. (In German.)

Cain, P. 1978. Measurements within self-aerated flow on a large spillway. Ph.D. thesis, Ref. 78-18, Department of Civil Engineering, University of Canterbury, Christchurch, New Zealand.

Chamani, M.R. 2000. Air inception in skimming flow regime over stepped spillways. *In* Proceedings of the International Workshop on Hydraulics of Stepped Spillways, Zürich, Switzerland. *Edited by* H.E. Minor and W.H. Hager. A.A. Balkema, Rotterdam, The Netherlands, pp. 61–67.

Chamani, M.R., and Rajaratnam, N. 1999. Characteristics of skimming flow over stepped spillways. ASCE Journal of Hydraulic Engineering, **125**(4): 361–368.

Chanson, H. 1993*a*. Stepped spillway flows and air entrainment. Canadian Journal of Civil Engineering, **20**(3): 422–435.

Chanson, H. 1993*b*. Self-aerated flows on chutes and spillways. ASCE Journal of Hydraulic Engineering, **119**(2): 220–243. Discussion: **120**(6): 778–782.

Chanson, H. 1995*a*. Hydraulic design of stepped cascades, channels, weirs and spillways. Pergamon, Oxford, U.K.

Chanson, H. 1995*b*. Air bubble diffusion in supercritical open channel flow. *In* Proceedings of the 12th Australasian Fluid Mechanics Conference AFMC, Sydney, Australia. *Edited by* R.W. Bilger. Vol. 2, pp. 707–710.

Chanson, H. 1996. Prediction of the transition nappe/skimming flow on a stepped channel. Journal of Hydraulic Research, IAHR, **34**(3): 421–429.

Chanson, H. 1997*a*. A short history of stepped cascades in Australia. ANCOLD Bulletin, No. 106, August, pp. 101–111.

Chanson, H. 1997*b*. Air bubble entrainment in free-surface turbulent shear flows. Academic Press, London, U.K.

Chanson, H. 2000. Forum article. Hydraulics of stepped spillways. ASCE Journal of Hydraulic Engineering, **126**(9): 636–637.

Chanson, H., and Brattberg, T. 1998. Air entrainment by two-dimensional plunging jets: the impingement region and the very-near flow field. Proceedings of the 1998 ASME Fluids Engineering Conference, FEDSM'98, Washington, D.C., 21–25 June, Paper FEDSM98-4806, CD-ROM.

Chanson, H., and Toombes, L. 2001. Experimental investigations of air entrainment in transition and skimming flows down a stepped chute. Application to embankment overflow stepped spillways. Research Report No. CE158, Department of Civil Engineering, The University of Queensland, Brisbane, Australia.

Chanson, H., and Whitmore, R.L. 1998. Gold Creek dam and its unusual waste waterway 1890–1997): design, operation, and maintenance. Canadian Journal of Civil Engineering, **25**(4): 755–768.

Chanson, H., Yasuda, Y., and Ohtsu, I. 2000. Flow resistance in skimming flow: a critical review. *In* Proceedings of the International Workshop on Hydraulics of Stepped Spillways, Zürich, Switzerland. *Edited by* H.E. Minor and W.H. Hager. A.A. Balkema, Rotterdam, The Netherlands, pp. 95–102.

Crowe, C., Sommerfield, M., and Tsuji, Y. 1998. Multiphase flows with droplets and particles. CRC Press, Boca Raton, Fla.

Frizell, K.H. 1992. Hydraulics of stepped spillways for RCC dams and dam rehabilitations. Proceedings of the 3rd Specialty Conference on Roller Compacted Concrete, American Society of Civil Engineers, San Diego, Calif., pp. 423–439.

Haugen, H.L., and Dhanak, A.M. 1966. Momentum transfer in turbulent separated flow past a rectangular cavity. Journal of Applied Mechanics, Transactions ASME, September, pp. 641–646.

Henderson, F.M. 1966. Open channel flow. MacMillan Company, New York.

Horner, M.W. 1969. An analysis of flow on cascades of steps. Ph.D. thesis, University of Birmingham, U.K.

Kelen, N. 1933. Gewichtsstaumauern und Massive Wehre. Verlag von Julius Springer, Berlin, Germany. (In German.)

Matos, J. 2000. Hydraulic design of stepped spillways over RCC dams. *In* Proceedings of the International Workshop on Hydraulics of Stepped Spillways, Zürich, Switzerland. *Edited by* H.E. Minor and W.H. Hager. A.A. Balkema, Rotterdam, The Netherlands, pp. 187–194.

Ohtsu, I., and Yasuda, Y. 1997. Characteristics of flow conditions on stepped channels. Proceedings of the 27th IAHR Biennial Congress, San Francisco, Calif., Theme D, pp. 583–588.

Rajaratnam, N. 1990. Skimming flow in stepped spillways. ASCE Journal of Hydraulic Engineering, **116**(4): 587–591. Discussion: **118**(1): 111–114.

Rouse, H. 1937. Modern conceptions of the mechanics of turbulence. ASCE Transactions, **102**: 463–543.

Ruff, J.F., and Frizell, K.H. 1994. Air concentration measurements in highly-turbulent flow on a steeply-sloping chute. Proceedings of the American Society of Civil Engineers Hydraulic Engineering Conference, Buffalo, N.Y., Vol. 2, pp. 999–1003.

Schlichting, H. 1979. Boundary layer theory. 7th ed. McGraw-Hill, New York, N.Y.

Schuyler, J.D. 1909. Reservoirs for irrigation, water-power and domestic water supply. 2nd ed. John Wiley & Sons, New York, N.Y.

Shvainstein, A.M. 1999. Stepped spillways and energy dissipation. Gidrotekhnicheskoe Stroitel'stvo, No. 5, pp. 15–21. (In Russian.) Also in Hydrotechnical Construction, **3**(5): 275–282.

Sumer, B.M., Cokgor, S., and Fredsoe, J. 2001. Suction removal of sediment from between armor blocks. ASCE Journal of Hydraulic Engineering, **127**(4): 293–306.

Toda, K., and Inoue, K. 1997. Advection and diffusion properties of air bubbles in open channel flow. *In* Proceedings of the 27th

IAHR Congress, San Francisco, Calif. *Edited by* F.M. Holly Jr. and A. Alsaffar. Theme B, Vol. 1, pp. 76–81.

Tozzi, M.J. 1992. Caracterização/Comportamento de Escoamentos em Vertedouros com Paramento em Degraus. (Hydraulics of stepped spillways.) Ph.D. thesis, University of Sao Paulo, Brazil. (In Portuguese.)

Tozzi, M., Taniguchi, E., and Ota, J. 1998. Air concentration in flows over stepped spillways. Proceedings of 1998 ASME Fluids Engineering Conference, FEDSM'98, Washington, D.C., 21–25 June, Paper FEDSM98-5053, CD-ROM.

Wegmann, E. 1907. The design of the new Croton dam. ASCE Transactions, Vol. LXVIII, No. 1047, pp. 398–457.

Wegmann, E. 1911. The design and construction of dams. 6th ed. John Wiley & Sons, New York, N.Y.

Wood, I.R. 1985. Air water flows. Proceedings of the 21st IAHR Congress, Melbourne, Australia, Keynote address, pp. 18–29.

Wood, I.R. 1991. Air entrainment in free-surface flows. Hydraulic design considerations. IAHR Hydraulic Structures Design Manual No. 4. A.A. Balkema, Rotterdam, The Netherlands.

Yasuda, Y., and Ohtsu, I. 1999. Flow resistance of skimming flow in stepped channels. Proceedings of the 28th IAHR Congress, Graz, Austria, Session B14, CD-ROM.

List of symbols

C air concentration defined as the volume of air per unit volume, also called void fraction
C_{mean} depth-averaged air concentration defined as $(1 - Y_{90})C_{mean} = d$
D_H hydraulic diameter (m); $D_H = 4dW/(W + 2d)$ for a rectangular channel
D_t turbulent diffusivity (m^2/s) of air bubble in air–water flows
D_o dimensionless coefficient
D' dimensionless air bubble diffusivity (Appendix 1)
d characteristic depth (m) defined as $d = \int_0^{Y_{90}} (1 - C)\,dy$
d_c critical flow depth (m); for a rectangular channel, $\sqrt[3]{q_w^2/g}$
F_{ab} bubble count rate (Hz), i.e., number of bubbles detected by the probe sensor per second
$(F_{ab})_{max}$ maximum bubble count rate (Hz)
f Darcy friction factor
f_d equivalent Darcy friction factor estimate of the form drag
f_e Darcy friction factor of air–water flows
g gravity constant (m/s^2) or acceleration of gravity; g = 9.80 m/s^2 in Brisbane
h height of steps (m) (measured vertically)
K inverse of the spreading rate of a turbulent shear layer
K', K'', K''' integration constants
l horizontal length of steps (m) (measured perpendicular to the vertical direction)
N exponent of the velocity power law
Q discharge (m^3/s)
q discharge per unit width (m^2/s)
R normalized cross-correlation coefficient
S_f friction slope
s curvilinear coordinate (m) measured in the flow direction
s_I distance (m) of the inception point of free-surface aeration measured from the upstream crest edge
T bubble travel time (s) for which the cross-correlation function is maximum
Tu turbulence intensity defined as Tu = u'/V
Tu′ characteristic turbulence intensity in air–water flows (Appendix 2)
U_w clear-water flow velocity (m/s), $U_w = q_w/d$
u' root mean square of longitudinal component of turbulent velocity (m/s)
u_r bubble rise velocity (m/s)
$(u_r)_{Hyd}$ bubble rise velocity (m/s) in a hydrostatic pressure gradient
V velocity (m/s)
V_c critical velocity (m/s); for a rectangular channel, $V_c = \sqrt[3]{gq_w}$
V_{90} characteristic velocity (m/s) where the air concentration is 90%
W channel width (m)
x longitudinal distance (m)
y distance (m) from the pseudo-bottom (formed by the step edges) measured perpendicular to the flow direction
Y_{90} characteristic depth (m) where the air concentration is 90%
α channel slope
Δx distance between probe sensors (m)
ΔT time scale (s) for which the cross-correlation function equals half of its maximum
Δt characteristic time (s) for which the normalized autocorrelation function equals 0.5
λ dimensionless coefficient
ρ density (kg/m^3)
τ_o boundary shear stress (Pa)
Ø diameter (m)

Subscripts

c critical flow conditions
w water flow

Appendix 1. Air bubble diffusion in self-aerated flows (by H. Chanson)

In supercritical flows, free-surface aeration, also called white waters, occurs when turbulence acting next to the free surface is large enough to overcome both surface tension for the entrainment of air bubbles and buoyancy to carry downwards the bubbles. Assuming a homogeneous air–water mixture for $C < 90\%$, the advective diffusion of air bubbles may be analytically predicted at uniform equilibrium. The continuity equation for air in the air–water flow yields

$$[A1] \quad \frac{\partial}{\partial y}\left(D_t \frac{\partial C}{\partial y}\right) = \cos\alpha \frac{\partial}{\partial y}(u_r C)$$

where D_t is the turbulent diffusivity, u_r is the bubble rise velocity, α is the channel slope, and y is measured perpendicular to the mean flow direction. The bubble rise velocity in a fluid of density $\rho_w(1 - C)$ equals

$$[A2] \quad u_r^2 = [(u_r)_{Hyd}]^2(1 - C)$$

where $(u_r)_{Hyd}$ is the rise velocity in hydrostatic pressure gradient (Chanson 1995*b*, 1997*b*). A first integration of the continuity equation for air in the equilibrium flow region leads to

$$[A3] \quad \frac{\partial C}{\partial y'} = \frac{1}{D'} C\sqrt{1-C}$$

where $y' = y/Y_{90}$ and $D' = D_t/((u_r)_{Hyd} \cos \alpha\ Y_{90})$ is a dimensionless turbulent diffusivity. D' is the ratio of the air bubble diffusion coefficient to the rise velocity component normal to the flow direction times the characteristic transverse dimension of the shear flow.

Assuming a homogeneous turbulence across the flow (i.e., D' constant), the integration of eq. [A2] yields eq. [6], which was validated with smooth-invert chute model and prototype data (Chanson 1995*b*, 1997*b*). Advanced void fraction distribution models may be developed assuming a non constant diffusivity, i.e., eqs. [3] and [7]. Full details of integration were presented in Chanson and Toombes (2001).

For completeness, Toda and Inoue (1997) developed two-dimensional numerical models of the advective diffusion equation for air bubbles. The results of both Lagrangian and Eulerian models gave very similar results to air–water flow measurements and to the analytical models.

Appendix 2. Velocity measurements and cross-correlation techniques for dual-tip probe measurements in gas–liquid flows

In two-phase flows, a velocity measurement technique is based upon successive detection of bubbles/droplets by two sensors aligned in the flow direction. In highly turbulent air–water flows, the detection of a bubble by each probe sensor is highly improbable, and it is common to use a cross-correlation technique (Crowe et al. 1998). The time-averaged air–water velocity is defined as

$$[A4] \quad V = \frac{\Delta x}{T}$$

where Δx is the distance between probe sensors and T is the travel time for which the cross-correlation function is maximum. The shape of the cross-correlation function provides a further information on the turbulent velocity fluctuations. For example, flat cross-correlation functions are associated with large velocity fluctuations around the mean and large turbulence intensity $Tu = u'/V$, where u' is the standard deviation of the turbulent velocity fluctuations. The information must be corrected to account for the intrinsic noise of the leading probe signal and the turbulence intensity is related to the broadening of the cross-correlation function compared to the autocorrelation function.

Chanson and Toombes (2001) demonstrated that the turbulence intensity u'/V may be approximated as

$$[A5] \quad Tu = \frac{u'}{V} \approx 0.851 \frac{\sqrt{\Delta T^2 - \Delta t^2}}{T} = Tu'$$

where ΔT is a time scale for which the cross-correlation function equals half of its maximum (i.e., $R(T + \Delta T) = R(T)/2$) and Δt is the characteristic time for which the normalized autocorrelation function equals 0.5. Tu' is a dimensionless velocity scale that is characteristic of the turbulent velocity fluctuations over the distance Δx separating the probe sensors.